Pore-Filling Induced Solid Electrolyte Failure of Ti-Doped Na$_3$Zr$_2$Si$_2$PO$_{12}$ Characterized by *Operando* Synchrotron X-Ray Tomography**

Mengya Li,*[a] Marm Dixit,[a] Pavel Shevchenko,[b] Francesco De Carlo,[b] Mahalingam Balasubramanian,[a] and Ilias Belharouak*[a]

Solid-state batteries (SSBs), particularly those utilizing sodium metal, are emerging as a promising technology due to their potential for enhanced safety, higher energy density, and longer cycle life. NASICON (Na superionic conductor) materials, known for their robust crystalline structure and high ionic conductivity, are pivotal in the development of efficient sodium all-solid-state batteries. These materials exhibit high room-temperature ionic conductivity and electrochemical stability, making them ideal for various applications. Research has focused on improving NASICON's ionic conductivity and stability through doping, interface regulation, and composite anode design. Recent advancements include Ti-doped

Na$_3$Zr$_2$Si$_2$PO$_{12}$ (Ti-NZSP), which demonstrates improved surface stability, higher ionic conductivity, and increased critical current density. However, challenges such as Na dendrite formation and mechanical integrity under operational conditions persist. Advanced imaging techniques like *operando* synchrotron X-ray tomography have provided insights into failure mechanisms, revealing that pore-filling and dendrite growth are significant issues. Understanding these processes is essential for enhancing the performance and safety of Na-based SSBs. This study underscores the need for continued research to address these challenges and develop reliable, high-performance solid-state electrolytes for future energy storage solutions.

Introduction

The search for high-performance, safe, and sustainable energy storage systems has intensified with the growing demand for renewable energy integration and electric mobility. Sodium-ion batteries (SIBs) have emerged as a promising alternative to lithium-ion batteries (LIBs) due to the natural abundance, lower cost, and environmental friendliness of sodium.[1] Solid-state electrolytes (SSEs) have garnered significant attention for their potential to enhance the safety and performance of next-generation batteries.[2] Na-based SSBs hold the potential to revolutionize the energy storage landscape by offering several key advantages over their liquid-based counterparts. These

advantages include enhanced safety, improved energy density, and extended cycle life, all of which are essential for meeting the growing demands of electric vehicles, grid storage, and portable electronics.[3] However, realizing the full potential of Na-based SSBs requires a deep understanding of the complex processes that occur within these devices during operation, degradation, and failure.

NASICON, or Na superionic conductor, enables the development of cost-effective and safer sodium all-solid-state batteries.[4] NASICON materials are known for their robust crystalline structure and high Na+ mobility, which are critical for efficient energy storage and transfer. The high ionic conductivity of NASICON solid electrolytes is crucial for enhancing the performance of solid-state batteries.[5] One of the key advantages of Na-based NASICON solid-state batteries is their high room-temperature ionic conductivity and electrochemical stability, making them ideal for Na metal solid-state batteries.[6] Additionally, NASICON-based solid-state batteries are recognized for their high safety standards and energy density, making them appealing for various applications.[7] Among the different Na-based solid electrolytes, NASICON-type Na$_3$Zr$_2$Si$_2$PO$_{12}$ has been reported as a stable solid-state electrolyte with high ionic conductivity, making it a promising candidate for solid-state battery applications.[3b] However, despite these promising characteristics, there remain challenges associated with the mechanical integrity and long-term stability of these electrolytes under operational conditions. Research efforts have focused on enhancing the ionic conductivity of NASICON solid electrolytes through strategies such as doping, interface regulation, and composite anode design. These approaches aim to improve the overall performance and

[a] M. Li, M. Dixit, M. Balasubramanian, I. Belharouak
Electrification and Energy Infrastructures Division, Oak Ridge National Laboratory, Oak Ridge, TN 37830, USA
E-mail: lim1@ornl.gov
belharouaki@ornl.gov

[b] P. Shevchenko, F. De Carlo
Advanced Photon Source, Argonne National Laboratory, Lemont, IL 60439, USA

Batteries & Supercaps

Research Article
doi.org/10.1002/batt.202400429

Chemistry Europe
European Chemical
Societies Publishing

stability of Na-based NASICON solid-state batteries by addressing factors like dendrite growth, interface impedance, and cycle stability.[8] In prior work by our team, we introduced TiO_2 into $Na_3Zr_2Si_2PO_{12}$ (Ti-doped $Na_3Zr_2Si_2PO_{12}$, or Ti-NZSP), which demonstrated significant improvements in the properties of the solid electrolyte (SE).[3b] Ti-NZSP exhibits lower porosity and more uniformly distributed pores, leading to stabilized surface properties, higher ionic conductivity, and an increased critical current density. These enhancements are particularly beneficial for solid-state battery applications, where dense SE and local structural stability are crucial for maintaining good Na+ conducting properties. The stable surface properties of Ti-NZSP ensure excellent interfacial properties, leading to stable electrochemical cycling performance and the ability to sustain high-rate electrochemical protocols. Despite these advancements, the failure mechanisms of Na symmetric cells using Ti-NZSP SE under extreme electrochemical conditions are not well understood.

Na dendrite formation in NASICON solid electrolytes has been a significant area of investigation in the realm of solid-state batteries. Gao et al. highlighted the challenges faced when using NASICON-based solid-state electrolytes in conjunction with metallic sodium, as they are prone to failure due to the growth of Na dendrites that propagate through the electrolyte during the plating process.[9] The presence of grain boundaries and microscopic defects in the bulk of the solid-state electrolyte, as well as issues with contact loss at the interface between the electrolyte and the metal, were identified as key factors contributing to dendrite growth. Moreover, Matios et al. pointed out that Na tends to plate preferentially along the grain boundaries of NASICON, where the Na + flux is locally intensified, leading to detrimental dendrite-like nucleation on the Na anode over repeated charge/discharge cycles.[8a] This phenomenon underscores the importance of understanding the microstructural features of NASICON that influence dendrite formation, emphasizing the need for strategies to mitigate this issue. Pervez et al. conducted postmortem studies confirming the presence of Na dendrites in the pores and along the grain boundaries of NASICON ceramic structures.[6] This observation further underscores the significance of addressing dendrite formation in NASICON solid electrolytes to enhance the performance and safety of solid-state batteries utilizing this material. Furthermore, Zhang et al. highlighted that the inhomogeneous current distribution induced by nonuniform interfacial connections between Na metal and solid-state electrolytes, along with factors such as the infinite volume change of Na metal and unreliable solid electrolyte interphase (SEI), play crucial roles in Na dendrite formation.[10] Understanding these mechanisms is essential for developing strategies to prevent dendrite growth and mitigate the risk of short circuits in solid-state batteries.

Understanding the failure mechanisms associated with solid electrolytes is essential for the design of more reliable and efficient batteries. In this study, we designed a customized cell system to characterize the cell under progressively intensified galvanostatic protocols using *operando* synchrotron X-ray tomography. Synchrotron X-ray tomography is an advanced imaging technique that utilizes the high-intensity, monochromatic X-rays produced by synchrotron radiation sources. It offers exceptionally high spatial resolution and contrast, allowing for detailed three-dimensional visualization of a material's internal structure < col[11] This advanced imaging technique allowed for detailed observation of structural changes within the SE during operation. Our findings revealed that cell failure is predominantly due to a pore-filling mechanism, where the formation of dead Na leads to enlarged pores and dendrite formation. These insights are crucial for developing better SE materials tailored for multiple applications, such as Na metal batteries and seawater batteries, ultimately paving the way for safer and more efficient energy storage solutions.

Experimental Details

Material Synthesis

Na3Zr2Si2PO12 powder was purchased from MSE Supplies. 2 wt% TiO2 powder (Sigma-Aldrich) was mixed with Na3Zr2Si2PO12 powder in a ball mill jar for one hour. Then 0.3 gram was added to a 12-mm diameter heated die for pressing at 200 °C for 30 min. The pellet was later annealed in a box furnace at 1000 °C for 24 hours. Prior to further cell assembly, the pellet was polished with 500 and 2500 grit sandpaper to ensure a reflective surface.

Electrochemical Testing

A customized *operando* cell was assembled inside an Argon glovebox with minimal oxygen and water ppm levels. Sodium metal disks, approximately 1.5 mm in diameter, were punched and used as electrodes in a symmetric cell configuration, with a Ti-NZSP pellet positioned between them. The cell was connected to a Gamry Reference 3000 electrochemical workstation to perform galvanostatic plating/stripping experiments, using gradually increasing current profiles as illustrated in Figure 1.

Characterization

The morphology and phase of the sintered Ti-NZSP pellet were confirmed by SEM and XRD in our previous work. *Operando* synchrotron X-ray tomography scans was carried out on Na | Ti-NZSP | Na symmetric cell at Advanced Photon Source at the Argonne National Laboratory Beamline 2-BM−B. Filtered pink with cut out at 30 keV was used to allow for penetration through the Ti-NZSP pellet in a Na symmetric cell. 1500 projections with an exposure time of 120 ms each were recorded evenly during 180° rotation of the sample. A Oryx ORX-10 G-51S5 M camera coupled with a 2x objective lens was used that gives a voxel size of ~1.5 μm and a total FoV of ~2.5×1 mm². Under these experimental conditions, a single tomographic scan took approximately 25 to 30 minutes. The raw data obtained was processed with TomocuPy.[12] The reconstructed images were binarized using auto thresholding routines available in Fiji/ImageJ. Porosity was evaluated for the entire solid electrolyte pellet with this routine to remove potential bias. Identical thresholds for binarization were used across all the samples for comparison. Pore size distribution plugin was used on the binarized image sets to identify distribution of pore sizes in the sample.[13] All subsequent image analysis was carried out with Fiji plugins or using custom-built MATLAB routines.
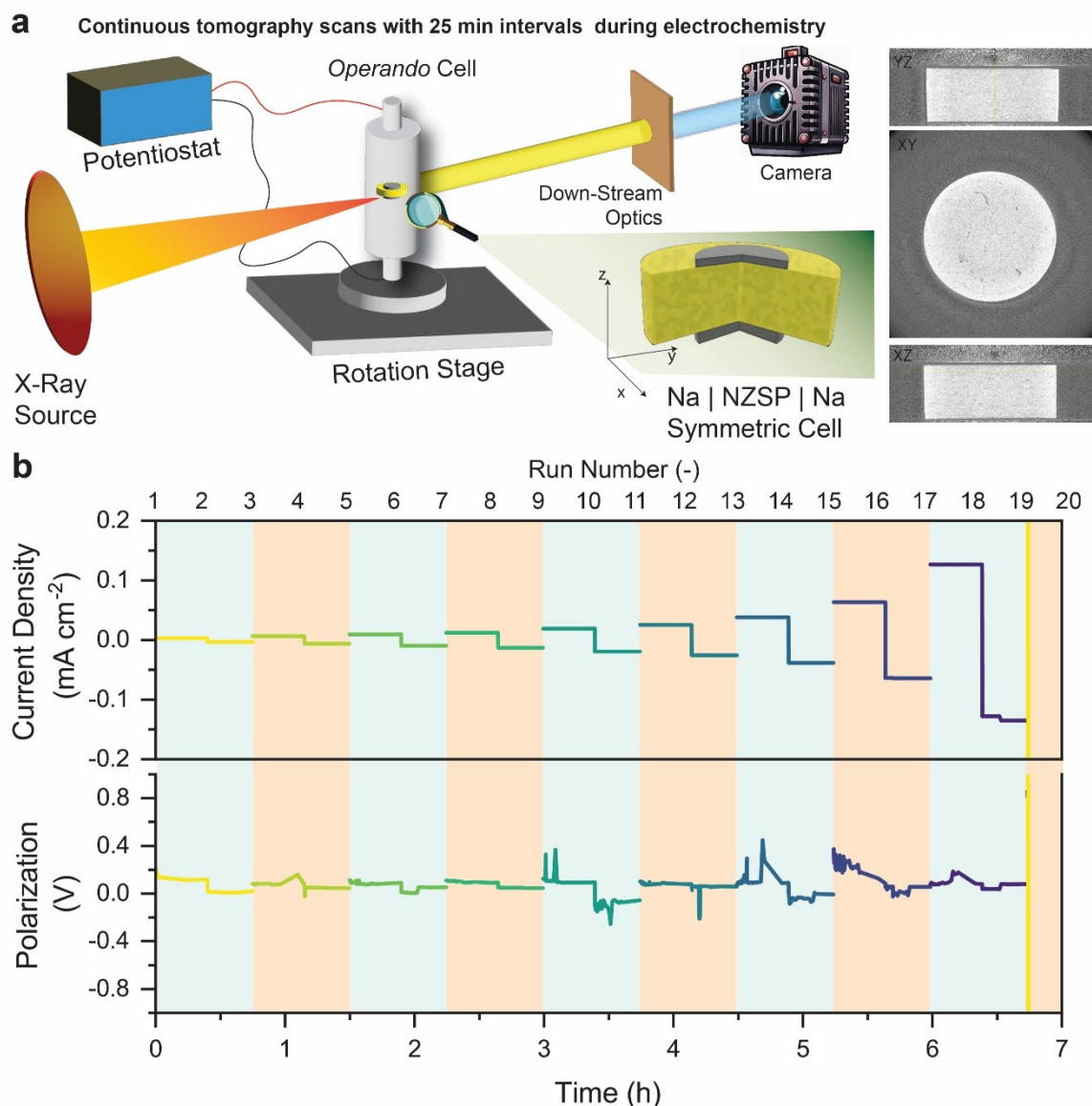
Figure 1. (a) Synchrotron X-ray tomography (μCT) set-up at APS beamline 2-BM for this work, with XY, YZ, XZ projections of the symmetric cell. Downstream optics consist of a scintillator and an objective lens. (b) Electrochemical testing protocol on the Na | Ti-NZSP | Na cell.

Results and Discussion

Operando synchrotron X-ray tomography was performed on Na | Ti-NZSP | Na cell, as depicted in the set-up scheme shown in Figure 1a. The inset provides a zoomed-in schematic illustration of the symmetric cell. Our research demonstrated that the introduction of TiO_2 into $Na_3Zr_2Si_2PO_{12}$ solid-electrolyte significantly improves its structural and chemical properties, resulting into enhanced electrochemical performance in both Na symmetric cell and Na || HC half-cell configurations.[3b] Although a much higher critical current density value of 2.5 mA cm^{-2} was reported, the exact cell failure mechanism remained unclear. To elucidate the failure mechanism of Ti-NZSP SE, we designed a galvanostatic electrochemical protocol with gradually increased current densities to intensify the failure process of the Na | Ti-NZSP | Na symmetric cell. The detailed protocol applied to the

symmetric cell is shown in Figure 1b. Continuous tomography scans were collected at 25-minute intervals throughout the entire electrochemical process, which lasted approximately 7 hours with a total of 20 tomography scans (labelled with run #). Note that the Run 1 was carried out before starting electrochemical testing, while run 20 was carried out after the failure of the cell. The cell was cycled at increasingly higher current densities ranging from ~0.01 mA cm^{-2} all the way up to ~0.15 mA cm^{-2}. This kind of electrochemical protocol has previously been employed for *operando* cells for tomography measurements.[14] In the initial stages, the polarization response is flat for low applied current density indicating a planar Na metal deposition in both plating and stripping stages. As the applied current density is increased, the voltage profile becomes erratic and shows increase within a single plating or stripping cycle. This polarization response is consistent with
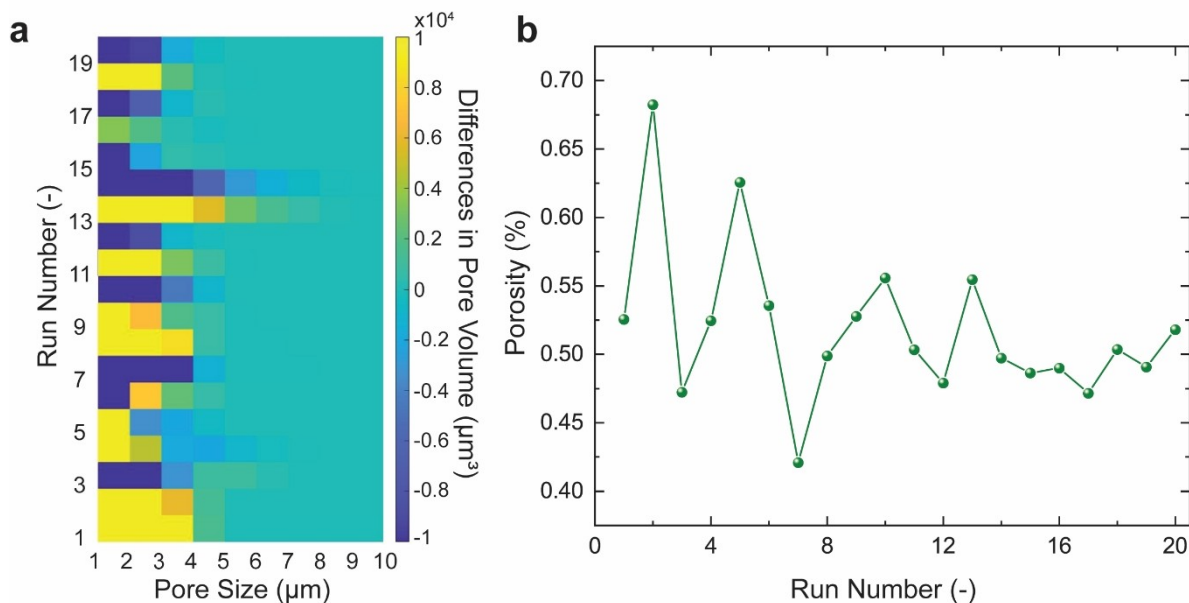
Figure 2. (a) Pore size evolution and changes in pore volume and (b) porosity changes within the Ti-NZSP solid electrolyte during the applied electrochemical protocols.
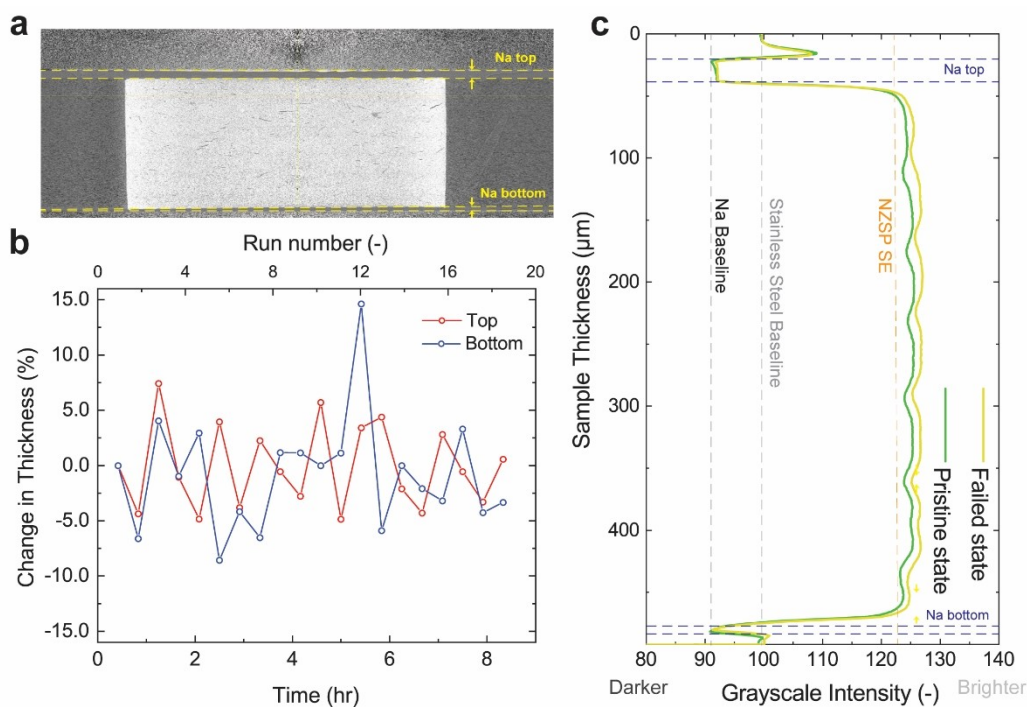

Figure 3. (a) Cross-sectional X-ray tomography image of the Na | Ti-NZSP | Na symmetric cell. (b) Evolution of Na thickness upon electrochemical testing. (c) Grayscale intensity values of the Ti-NZSP SE on the cross-section.

void formation at the Na | NASICON interface as well as formation of filament within the cell as reported previously.[14,15] After four plating and stripping cycles, the cell potential shows non-linear behavior with jumps in potential, indicating a significant deterioration of the interface and a large interfacial resistance. We continued our cycling approach where increasingly higher currents were applied until a large current and short were observed (~6.5 h mark) on the cell. Subsequent cycling of the cell shows negligible current flowing through the cell indicating a clear failure.
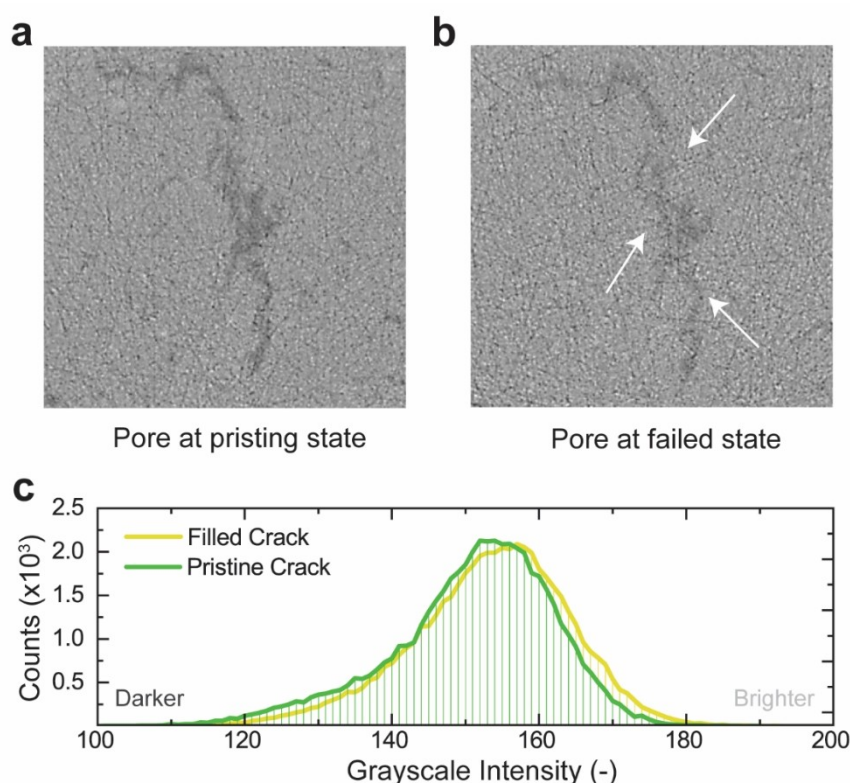
Batteries & Supercaps

Research Article
doi.org/10.1002/batt.202400429

Chemistry
Europe
European Chemical
Societies Publishing

Figure 4. Grayscale images of a porous region on the Ti-NZSP SE (a) at the pristine state (run #. 1) and (b) at the failed state (run #20). (c) Histogram comparison of grayscale intensity values of pore/cracked at the pristine and failed state.

Image reconstruction was performed for all the tomography datasets obtained during *operando* measurements from the pristine state to the failed state of the symmetric cell. Information regarding pore volume, pore size distribution, and Na thickness was analyzed in Fiji/ImageJ and custom-built MATLAB routines. The evolution of pore size versus run number is illustrated in the color-coded contour plot in Figure 2a. The pore size distribution for the stack is determined from binarized images. The identified pore spaces are classified into regions based on the size of balls that can fill them, with each region corresponding to a different radius. These radii are then assigned to their respective locations. The resulting histogram of these radii provides a continuous pore size distribution.[16] We illustrate the changes in the measured pore size distributions at each step of the tomography scans (Figure 2a). These difference values reflect alterations in the internal microstructure of the NZSP pellet, with consistent reconstruction and thresholding routines applied across all steps. During the cycling steps, we clearly see a cyclical variation in pore size distributions indicating that the Na$^+$ starts to plate and strip through the Ti-NZSP reversibly under the electrochemical protocol initially. However, by run number 13, larger pores begin to appear, and the pore volume for each pore size continuously decreases instead of fluctuating reversibly. Changes in the porosity of the Ti-NZSP can be found in Figure 2b, where the total porosity exhibits a clear damping trend across all run numbers, from the pristine to the failed state. Interestingly, the final porosity is similar to the initial

value (~0.52%). This behavior is different from the trends observed for LLZO solid electrolytes or sulfide solid electrolytes in Li metal batteries which show a consistent increase in the porosity upon failure. The Li filament growth in these electrolytes leads to crack formation, and generally, the Li cannot be distinguished from the pores within the bulk of the solid electrolyte.[14,15b,17] This results in a consistent increase in porosity from pristine to the failed state. However, as will be discussed later, Na filament growth within the electrolytes leads to an increase in the grayscale value of the pore-resulting in them not being picked up with the binarization. This behavior is distinct and likely only observed with these NASICON solid electrolytes.

The cross-sectional view of the Na | Ti-NZSP | Na cell tomography image is shown in Figure 3a. The regions between the highlighted dashed lines correspond to the top and bottom Na disks. In addition to analyzing tomography images of the Ti-NZSP pellet, we also performed analysis of the two Na disks. The thickness of each Na disk was measured by averaging five measurements taken along the full width of the disk. The changes in the thickness of the top and the bottom disks throughout the electrochemical process are plotted in Figure 3b. From run number 4, the top and bottom thicknesses began to show opposite trends, indicating an initial reversible plating/stripping process. By run number 12, the changes in the thickness of the top and the bottom Na disks polarized, reflecting an asymmetrical trend. This phenomenon could be attributed to an irreversible pore-filling process by Na$^+$ into the

Initial plating

Na$^+$

Initial stripping

Na$^+$

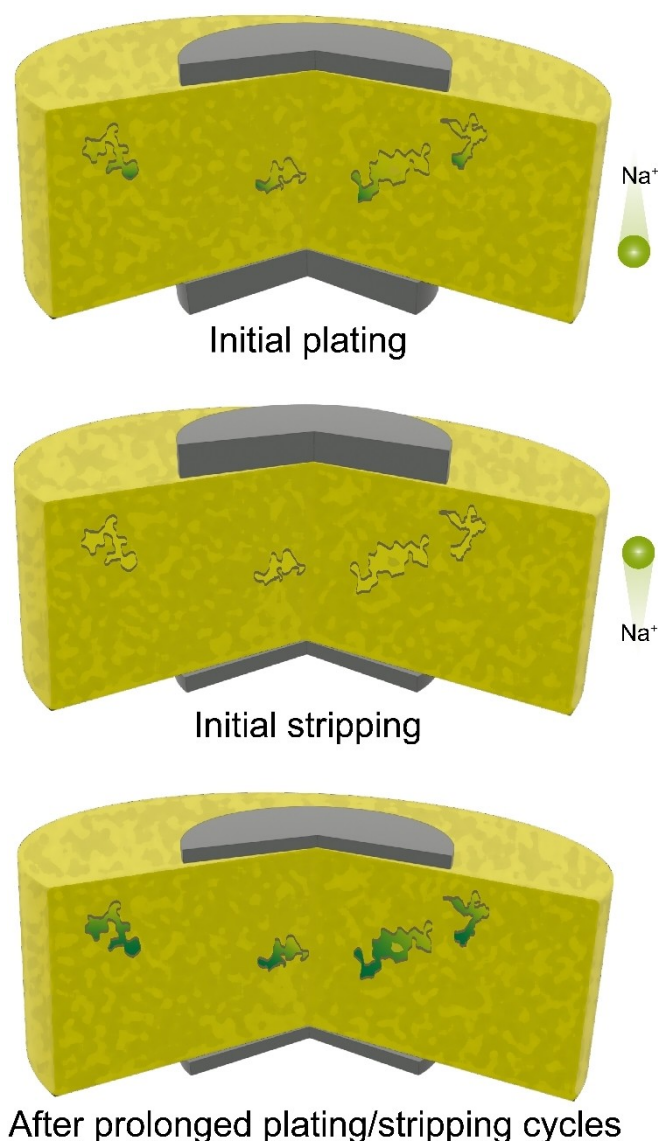After prolonged plating/stripping cycles

Figure 5. Schematic illustration of the cell failure mechanism associated with the irreversible pore filling by Na after prolonged plating/stripping cycles.

pores of Ti-NZSP, followed by the formation of dead Na in some of the pores. Figure 3c shows a vertical view of the cross-sectional image. With careful grayscale analysis, we defined baselines for Na metal and stainless steel and found that the overall grayscale intensities of the Ti-NZSP SE are higher in the failed state compared to the pristine state. It is worth noticing that although the grayscale intensity of Na disk (highlighted between the navy dashed lines in Figure 3c) remains the lowest, the grayscale intensity of pores filled with Na should be brighter than that of standalone pores. Therefore, after cell failure, the overall area of interest became brighter, which can be correlated to Na filling the pores inside Ti-NZSP SE. This is consistent with the observation about porosity trends discussed earlier.

A representative porous region was selected from the exact same slice number of Ti-NZSP at both the pristine and the failed states for direct comparison (Figures 4a and b). Following the

cell failure, the previously dark porous region became brighter, indicative of pore filling with Na deposits. The overall grayscale intensity distribution histogram of the area of interest was compared in Figure 4c for both pristine and failed states (where filled crack is observed). The distribution shifted towards higher grayscale intensity values, corresponding to a brighter area, after cell failure or after irreversible pore/crack filling. We proposed a schematic illustration of the failure mechanism in Figure 5.

During initial plating, Na$^+$ from the top starts to fill the porous region and form Na metal deposits. Subsequently during stripping process, the Na deposit formed in the pores are removed as Na$^+$ and re-deposited onto the top sodium metal disk. The initial reversible process can occur iteratively until the system becomes sufficiently polarized under external high current or voltage bias. With prolonged plating/stripping cycles under polarized electrochemical conditions, the Na metal deposits formed in the pores became inactive. From an electro-chemo-mechanical perspective, this polarization leads to uneven ion flux and mechanical stresses, exacerbating pore expansion and promoting the formation of dendrites.[18] The stress is especially concentrated at regions with mechanical heterogeneity, such as the interface between the solid electrolyte and Na metal, where uneven deposition of Na can lead to localized high-stress regions. These stresses can surpass the mechanical strength of the solid electrolyte, causing crack formation and propagation, further destabilizing the system. This interplay between electrochemical reactions and mechanical deformation not only accelerates the degradation of the solid electrolyte but also contributes significantly to the overall failure of the cell, as the continued accumulation of mechanical stress and uneven electrochemical activity lead to the eventual short-circuiting and failure of the battery.

Conclusions

This study provides critical insights into the failure mechanisms of Ti-doped Na$_3$Zr$_2$Si$_2$PO$_{12}$ (Ti-NZSP) solid electrolytes in Na symmetric cells under extreme electrochemical conditions. By employing *operando* synchrotron X-ray tomography, we were able to observe the evolution of structural changes within the solid electrolyte during operation. The findings reveal that the failure of the Na | Ti-NZSP | Na cell is predominantly due to a pore-filling mechanism. Initially, Na$^+$ ions fill the pores of Ti-NZSP during plating, and during stripping, the Na deposits are removed, leading to an irreversible increase in pore volume and the formation of dead Na. This process eventually results in the expansion of pores and the formation of Na dendrites, which cause short-circuiting and cell failure. Our detailed analysis demonstrated that the porosity of the Ti-NZSP SE changes significantly throughout the electrochemical process. Initially, the pore volume undergoes reversible changes, but as the process progresses, the formation of larger pores and the continuous decrease in pore volume indicate a transition to irreversible pore filling. The increase in overall grayscale intensity in the tomography images further supports the

conclusion that Na fills the pores within the Ti-NZSP, leading to failure. This study highlights the importance of understanding and mitigating pore-filling mechanisms to enhance the reliability and performance of solid-state electrolytes.

In conclusion, the insights gained from this work underscore the necessity for designing solid electrolytes with improved structural properties to prevent pore filling and dendrite formation. These findings pave the way for the development of more robust and efficient solid-state batteries. Future research should focus on optimizing the composition and structure of Ti-NZSP to enhance its resistance to pore-filling and dendrite formation, ensuring long-term stability and high performance in various battery applications.

Conflict of Interests

The authors declare no conflict of interest.

Data Availability Statement

The data that support the findings of this study are available from the corresponding author upon reasonable request.

[1] a) E. Goikolea, V. Palomares, S. Wang, I. R. de Larramendi, X. Guo, G. Wang, T. Rojo, *Adv. Energy Mater.* **2020**, *10*, 2002055; b) D. Larcher, J.-M. Tarascon, *Nat. Chem.* **2015**, *7*, 19; c) T. Liu, Y. Zhang, C. Chen, Z. Lin, S. Zhang, J. Lu, *Nat. Commun.* **2019**, *10*, 1965

[2] a) J. Wan, J. Xie, D. G. Mackanic, W. Burke, Z. Bao, Y. Cui, *Mater. Today Nano.* **2018**, *4*, 1; b) Q. Zhao, S. Stalin, C.-Z. Zhao, L. A. Archer, *Nat. Rev. Mater.* **2020**, *5*, 229

[3] a) L. Shen, J. Yang, G. Liu, M. Avdeev, X. Yao, *Mater. Today Energy* **2021**, *20*, 100691; b) M. Li, M. Dixit, R. Essehli, C. J. Jafta, R. Amin, M. Balasubramanian, I. Belharouak, *Adv. Sci.* **2023**, *10*, 2300920

[4] M. Samiee, B. Radhakrishnan, Z. Rice, Z. Deng, Y. S. Meng, S. P. Ong, J. Luo, *J. Power Sources* **2017**, *347*, 229.

[5] Y. Liu, J. Liu, Q. Sun, D. Wang, K. R. Adair, J. Liang, C. Zhang, L. Zhang, S. Lu, H. Huang, *ACS Appl. Mater. Interfaces* **2019**, *11*, 27890.

[6] S. A. Pervez, E. P. Roberts, M. Trifkovic, *Energy Technol.* **2022**, *10*, 2200658.

[7] Z. Wang, Z. Wang, M. Li, C. Tang, K. Yu, P. Lv, W. Wei, *Solid State Ionics* **2023**, *396*, 116229.

[8] a) E. Matios, H. Wang, C. Wang, X. Hu, X. Lu, J. Luo, W. Li, *ACS Appl. Mater. Interfaces* **2019**, *11*, 5064; b) H. Fu, Q. Yin, Y. Huang, H. Sun, Y. Chen, R. Zhang, Q. Yu, L. Gu, J. Duan, W. Luo, *ACS Materials Lett.* **2019**, *2*, 127; c) W. Wang, W. Yuan, Z. Zhao, D. Zou, P. Zhang, Z. Shi, J. Weng, P. Zhou, *J. Electroanal. Chem.* **2023**, *937*, 117405.

[9] Z. Gao, J. Yang, G. Li, T. Ferber, J. Feng, Y. Li, H. Fu, W. Jaegermann, C. W. Monroe, Y. Huang, *Adv. Energy Mater.* **2022**, *12*, 2103607.

[10] Q. Zhang, Y. Lu, W. Guo, Y. Shao, L. Liu, J. Lu, X. Rong, X. Han, H. Li, L. Chen, *Energy Mater. Adv.* **2021**, *2021*, 9870879.

[11] a) S. Dayani, H. Markötter, J. K. von Nidda, A. Schmidt, G. Bruno, *Adv. Mater. Technol.* **2024**, *9*, 2301246; b) O. O. Taiwo, D. P. Finegan, J. Paz-Garcia, D. S. Eastwood, A. Bodey, C. Rau, S. Hall, D. J. Brett, P. D. Lee, P. R. Shearing, *Phys. Chem. Chem. Phys.* **2017**, *19*, 22111.

[12] V. Nikitin, *J. Synchrotron Radiat.* **2023**, *30*, 179.

[13] B. Münch, P. Gasser, L. Holzer, R. Flatt, *J. Am. Ceram. Soc.* **2006**, *89*, 2586.

[14] F. Shen, M. B. Dixit, X. Xiao, K. B. Hatzell, *ACS Energy Lett.* **2018**, *3*, 1056.

[15] a) K. N. Wood, E. Kazyak, A. F. Chadwick, K.-H. Chen, J.-G. Zhang, K. Thornton, N. P. Dasgupta, *ACS Cent. Sci.* **2016**, *2*, 790; b) M. B. Dixit, A. Verma, W. Zaman, X. Zhong, P. Kenesei, J. S. Park, J. Almer, P. P. Mukherjee, K. B. Hatzell, *ACS Appl. Energ. Mater.* **2020**, *3*, 9534

[16] B. Münch, L. Holzer, *J. Am. Ceram. Soc.* **2008**, *91*, 4059.

[17] M. B. Dixit, M. Regala, F. Shen, X. Xiao, K. B. Hatzell, *ACS Appl. Mater. Interfaces* **2018**, *11*, 2022.

[18] a) J. Lu, S. Zhang, J. Yao, Z. Guo, M. Osenberg, A. Hilger, H. Markötter, F. Wilde, I. Manke, X. Zhang, *ACS Nano.* **2024**, *18*, 10930; b) Y. Zheng, S. Zhang, J. Ma, F. Sun, M. Osenberg, A. Hilger, H. Markötter, F. Wilde, I. Manke, Z. Hu, *Sci. Bull.* **2023**, *68*, 813; c) F. Sun, C. Wang, M. Osenberg, K. Dong, S. Zhang, C. Yang, Y. Wang, A. Hilger, J. Zhang, S. Dong, *Adv. Energy Mater.* **2022**, *12*, 2103714